J|A|C|S
ARTICLES
Published on Web 11/01/2005

Geometry, Phase Stability, and Electronic Properties of Isolated Selenium Chains Incorporated in a Nanoporous Matrix

Irene Ling Li,[†] Jian Pang Zhai,[‡] Pascale Launois,[§] Shuang Chen Ruan,[†] and Zi Kang Tang*,[‡]

Contribution from the School of Engineering and Technology, Shenzhen University, China, Department of Physics, Hong Kong University of Science and Technology, Clear Water Bay, Kowloon, Hong Kong, and Laboratoire de Physique des Solides (UMR CNRS 8502), Bât. 510, Université Paris Sud, 91405 Orsay, France

Received June 5, 2005; E-mail: phzktang@ust.hk

Abstract: We report the fabrication process of isolated one-dimensional Se chains incorporated in the matrix of $AlPO_4$-5 single crystals and the experimental investigation of the geometry, phase stability, electronic properties, and electron−phonon coupling effect of these Se chains. The structure of the helical Se chains inside the channels is discussed on the basis of X-ray scattering measurements. Thermal analysis and temperature-dependent micro-Raman measurements show that Se single chains are flexible and can convert from a weak distorted phase into another phase with strongly disordered structure ("melting" state) around 340 K. Since the electrons are confined in the one-dimensional channels, the absorption band of the Se chain is obviously blue shifted compared with that of trigonal Se. With increasing temperature, this band shifts linearly to the lower energy side, in sharp contrast to the nonlinear temperature coefficient of trigonal Se, which is attributed to the greatly diminished interchain interaction and the weakening of the electron−optical phonon coupling in a low-dimensional system. In the vicinity of the absorption band, both first-order and second-order Raman signals for the Se chain are enhanced, due to the strong electron−phonon coupling when the excitation laser energy matches the electronic transition in isolated Se chains.

1. Introduction

Since its discovery in 1817, selenium has been studied extensively due to its special photovoltaic and photoconductive properties. It has technological applications in photocells, xerography, rectifiers, coloring of glasses, etc.[1] Se can crystallize in different allotropes, such as trigonal, monoclinic, and rhombohedral structures. The trigonal form (*t*-Se) is the only modification that is stable under ambient conditions. The crystal structure of trigonal Se consists of helical chains which spiral around axes parallel to the *c* axis and are arranged in a hexagonal array. The space group is $P3_{121}$ (D_3^4) or $P3_{221}$ (D_3^6), depending on the sense of rotation of the helical chains.[2] The monoclinic and rhombohedral forms consist of puckered Se_8 and Se_6 rings, respectively. The Se ring and helix are distinguished by the correlation between neighboring dihedral angles. Depending on this correlation, Se can have either trans (chain-based) or cis (ring-based) configurations, as shown in Figure 1a. The energy difference between these two configurations was estimated to be only 0.03 eV.[3] Thus, Se can easily make an amorphous (*a*-Se) phase because of the flexibility of dihedral angles in the chain. The *a*-Se is regarded as an assembly of disordered chains with random signs and magnitudes of the dihedral angles.[4]

It is of great interest to investigate the properties of isolated Se helices or rings since the properties of bulk Se are of a strong molecular nature. Becker et al. studied Se_5, Se_6, Se_7, and Se_8 clusters and their aggregates by photoelectron spectroscopy and reported that as the cluster size increases the photoelectron spectra converge to that of the amorphous solid.[5] Ikawa et al. theoretically investigated the lattice structure and the electronic and vibronic properties of a single Se chain.[6−9] Endo et al. studied the ground-state properties and photoinduced effects of isolated chains enclosed in the channels of mordenite.[10] Poborchii et al. showed the vibration mode of the Se chain at 259 cm^{-1} for Se-loaded $AlPO_4$-5 crystals ($Se/AlPO_4$-5) and 256 cm^{-1} for Se-loaded mordenite crystals.[11,12] Kodaira et al. investigated the absorption spectra of $Se/AlPO_4$-5 crystals and found that with high loading density, Se mainly self-assembled

[†] Shenzhen University.
[‡] Hong Kong University of Science and Technology.
[§] Université Paris Sud.

(1) Cooper, W. C., Ed. *The Physics of Selenium and Tellurium*; Pergamon: Oxford, 1969.
(2) Bradley, A. J. *Philos. Mag.* **1924**, *48*, 477.
(3) Misawa, M.; Suzuki, K. *J. Phys. Soc. Jpn.* **1978**, *44*, 1612.
(4) Gerlach, E., Grosse, P., Eds. *The Physics of Selenium and Tellurium*; Springer-Verlag: New York, 1979.
(5) Becker, J.; Rademann, K.; Hensel, F. *Z. Phys. D* **1991**, *19*, 233.
(6) Ikawa, A.; Fukutome, H. *J. Phys. Soc. Jpn.* **1989**, *58*, 4517−4533.
(7) Ikawa, A.; Fukutome, H. *J. Phys. Soc. Jpn.* **1990**, *59*, 1002−1016.
(8) Ikawa, A.; Fukutome, H. *J. Non-Cryst. Solids* **1990**, *117/118*, 328−331.
(9) Nakamura, K.; Ikawa, A. *Phys. Rev. B* **2002**, *66*, 024306/1−13.
(10) Katayama, Y.; Yao, M.; Ajiro, Y. *J. Phys. Soc. Jpn.* **1989**, *58*, 1811−1822.
(11) Poborchii, V. V. *Chem. Phys. Lett.* **1996**, *251*, 230.
(12) Poborchii, V. V.; Kolobov, A. V.; Caro, J.; Zhuravlev, V. V.; Tanaka, K. *Chem. Phys. Lett.* **1997**, *280*, 17−23.

10.1021/ja053686+ CCC: $30.25

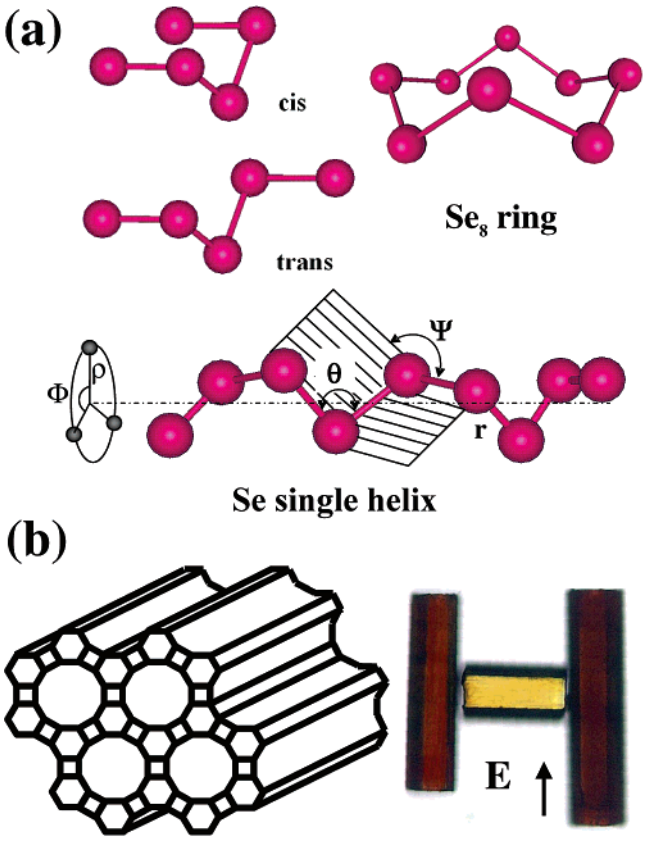

Figure 1. (a) Schematic representation of trans and cis configurations, as well as the ball-and-stick model, for a Se helix and ring. (b) Framework structure of the $AlPO_4$-5 single crystal (left) and optical microscopic view of a Se/$AlPO_4$-5 crystal (right) with polarized transmitted electric field.

into chain-like structures.[13,14] These works provide us microscopic information on the structure and ground state of isolated Se chains confined in a nanoporous matrix; however, information on other features, such as the detailed lattice parameters and electron−phonon coupling effect, in isolated Se chains is still limited.

In this article, we report the detailed fabrication process of isolated one-dimensional Se chains incorporated in the channels of $AlPO_4$-5 single crystals and the experimental investigation of the geometry, phase stability, and electronic and electron−phonon coupling properties of these Se chains. Single-crystal X-ray scattering experiments show diffuse planes attributed to scattering from helical selenium chains with their long axis parallel to the channel direction. Possible parameters of the Se chain can be deduced from these experiments: interatomic distance $r \approx 2.38$ Å, bond angle $\theta \approx 121°$, and dihedral angle $\psi \approx 42°$. Thermogravimetry (TG), differential scanning calorimetry (DSC), and temperature-dependent micro-Raman measurements show that isolated Se chains are flexible and can convert from a weak distorted phase into another phase with strongly disordered structure ("melting" state). The transformation temperature is about 340 K. Since the electrons are confined in the one-dimensional channels of $AlPO_4$-5 crystals, the absorption band of Se chain is obviously blue shifted compared with that of *t*-Se. With increasing temperature, this band shifts to the lower energy side linearly, in sharp contrast to the nonlinear temperature coefficient in *t*-Se. The distinct temperature behavior of the absorption band is attributed to the greatly diminished interchain interaction in Se/$AlPO_4$-5 and the weakening of the electron−optical phonon coupling in a low-dimensional system. The intensities of Raman active modes for helical Se chains are enhanced in the vicinity of the absorption band, which is attributed to a *resonant Raman effect*.

2. Experimental Section

Bulk Se has a low melting point (490 K) and a high vapor pressure; thus, Se species can be introduced into the $AlPO_4$-5 channels by a physical diffusion method. The $AlPO_4$-5 crystals used in our experiments were synthesized using an aqueous hydrothermal method.[15] The framework is constructed of alternative tetrahedra of AlO_4 and PO_4. They form parallel open one-dimensional channels arrayed in a hexagonal structure with space group *P*6*cc*. Figure 1b (left) shows the framework structure. The inner diameter of the channel is 7.3 Å, and the separation distance between two neighboring channels is 13.7 Å.

The selenium species were incorporated into the $AlPO_4$-5 crystal channels as follows: The $AlPO_4$-5 crystals were calcined at 560 °C in O_2 atmosphere for about 10 h to remove the organic tripropylamine molecules in the channels, thus emptying the channels. The calcined zeolite crystals were then sealed together with pure Se in a Pyrex tube in a vacuum of 10^{-1} Pa. Se was introduced to the channels by physical adsorption at 280 °C for around 48 h. The saturated Se-loaded crystals were orange, while the calcined $AlPO_4$-5 crystals were transparent. The crystal behaved as a good polarizer with high absorption for the light polarized parallel to the *c*-axis of the crystal, as shown in Figure 1b (right). This anisotropic optical property implies that an ordered selenium species with a large aspect ratio was formed along the channel.

X-ray scattering experiments were performed with a rotating anode at room temperature, using monochromatic Cu Kα radiation (λ = 1.5418 Å). The data were recorded under vacuum to optimize the signal/background ratio, on cylindrical X-ray films or imaging plates. Thermal analysis was carried out by using an STA 449C Jupiter apparatus. The mass resolution of the equipment is 0.1 μg. TG and DSC curves were taken simultaneously. Raman scattering experiments were performed using a backscattering geometry. The spectra were recorded by using a Jobin-Yvon T64000 Raman spectroscope equipped with a CCD detector cooled by liquid nitrogen. Up to 10 lines generated by an Innova 70C series ion laser and a He−Ne laser were used for excitation of the spectra. The wavelength of the monochromator is calibrated using a standard mercury lamp, and the detection sensitivities of the system at different wavelengths are calibrated using a quartz−tungsten−halogen irradiation source.

3. Results and Discussion

3.1. Structural Characterization. Figure 2 shows the energy-dispersive X-ray (EDX) pattern of an empty $AlPO_4$-5 and a Se/$AlPO_4$-5 single crystal. Both signals are taken from the cross section of the samples. The signals in the upper graph centered at 0.54, 1.48, and 2.06 keV distinguish the elements O, Al, and P contained in the $AlPO_4$-5 framework. In the bottom graph, an additional signal at 11.18 keV confirms the existence of Se species inside channels of the $AlPO_4$-5 crystals.

The X-ray scattering pattern for a Se/$AlPO_4$-5 single crystal is shown in Figure 3a. We can observe strong diffuse planes perpendicular to c^* at $Q_z = 0$ and $Q_z \approx \pm 2\pi/6.45$ Å^{-1}. X-ray scattering patterns measured on several empty $AlPO_4$-5 crystals did not show such diffuse planes.[16] They are thus characteristic

(13) Nozue, Y.; Kodaira, T.; Terasaki, O.; Yamazaki, K.; Goto, T.; Watanabe, D.; Thomas, J. M. *J. Phys.: Condens. Matters* **1990**, *2*, 5209−5217.
(14) Kodaira, T.; Ivanova, M. S.; Kiyozumi, Y.; Takeo, H.; Yamamoto, T.; Poborchii, V. V. *Trans. Mater. Res. Soc. Jpn.* **1996**, *20*, 470.
(15) Qiu, S.; Pang, W.; Kessler, H.; Guth, J. L. *Zeolites* **1989**, *9*, 440.
(16) Launois, P.; Moret, R.; Le Bolloc'h, D.; Albouy, P. A.; Tang, Z. K.; Li, G. D.; Chen, J. *Solid State Commun.* **2000**, *116*, 99−103.

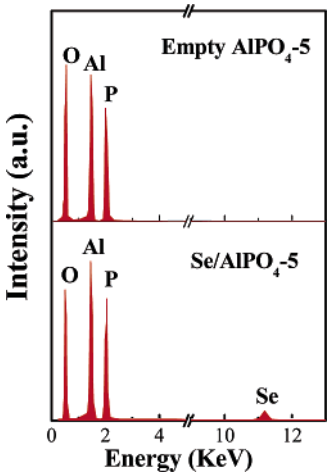

Figure 2. EDX pattern of a single empty $AlPO_4$-5 crystal (upper) and a single Se/$AlPO_4$-5 (bottom) crystal.

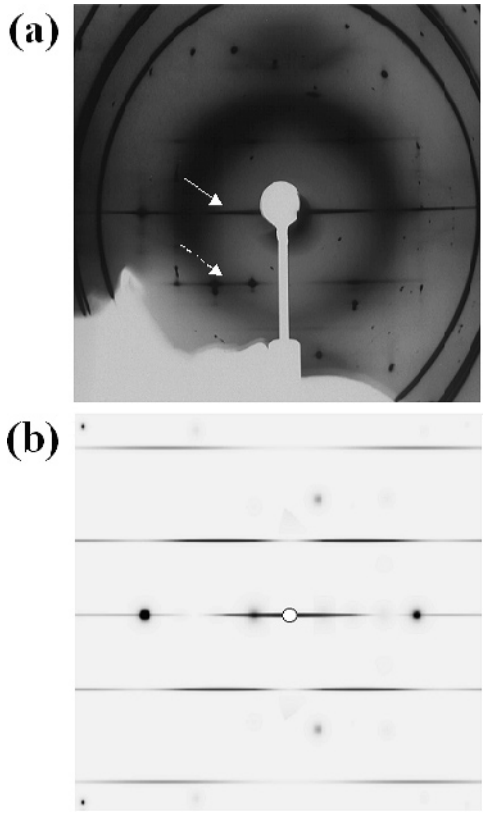

Figure 3. (a) X-ray scattering pattern for a Se/$AlPO_4$-5 single crystal. (b) Simulated patterns in rather good agreement with experiments.

of the Se/$AlPO_4$-5 crystals. Moreover, diffuse planes in reciprocal space correspond to disorder between periodic one-dimensional chains in direct space, and the observed diffuse planes can be related to periodic Se chains along the direction c of the $AlPO_4$-5 channels. The diffuse planes' width along c^* is resolution limited, which means that the chains are rather long (length > 200 Å; this value corresponds to the resolution). In the equatorial plane $Q_z = 0$, strong diffuse scattering is observed close to the origin. Such a feature, characteristic of substitutional disorder,[17] shows that the channels are not fully occupied by the Se chains, the filling rates differing from one

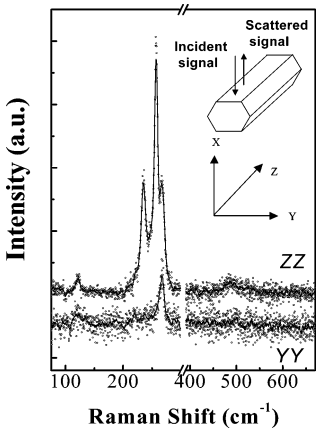

Figure 4. Polarized micro-Raman spectra for a Se/$AlPO_4$-5 single crystal in *ZZ* and *YY* configurations.

channel to the other. The distance between the diffuse planes and the positions of the other extrema of intensity within planes can be used to obtain the helix parameters.[18] Simulated patterns (Figure 3b) in rather good agreement with experiments are obtained for the following parameters: interatomic distance $r \approx 2.38$ Å, bond angle $\theta \approx 121°$, and dihedral angle $\psi \approx 42°$, which correspond to a helix radius $\rho \approx 1.7$ Å, a helix angle $\Phi \approx 2\pi/5$, and a translation along the helix axis $p \approx 1.29$ Å $= P/5$, where $P \approx 6.45$ Å is the period of the helix. These values differ from those calculated for an isolated Se chain (interatomic distance $r = 2.333$ Å, bond angle $\theta = 113.2°$, and dihedral angle $\psi = 77.2°$)[19] and those measured for a single chain incorporated inside the channels of mordenite (interatomic distance $r = 2.337$ Å, bond angle $\theta = 102°$, and dihedral angle $\psi = 75°$).[10] It is known that crystalline trigonal Se is the most stable form at ambient, but the single helical chain is flexible due to the absence of interchain interactions. Since the torsion energy barrier for a single chain is only 0.15 eV, the chain can easily be distorded.[19] The discrepancy between experimental and theoretical results indicated that the dihedral angle inside the isolated Se chains is considerably soft and can be easily altered by small perturbations. It should be noted that the helix radius deduced from our X-ray measurements $\rho = 1.7$ Å and the free channel diameter $D_f = 7.3$ Å are related by $D_f \approx 2(\rho + R_{vdW})$, where R_{vdW} is the Se van der Waals radius (1.9 Å). Thus, the Se helix fits its size to that of the $AlPO_4$-5 channels. This is not the case for helix radii in refs 19 and 10, where $\rho \approx$ 1.13 and 1.19 Å, respectively.

Since the single Se helix is structurally anisotropic, the study of polarized Raman spectra is important. Figure 4 shows the polarized Raman spectra of a Se/$AlPO_4$-5 crystal; the configuration for the measurement is shown in the inset. In the *ZZ* configuration (both the excitation and the scattering light are parallel to the crystal axis c), there are three strong Raman lines centered at 236, 258, and 267 cm^{-1}. They have been attributed to the first-order A_1 symmetric bond stretching modes of *t*-Se, the Se single helix, and the Se_8 ring, respectively.[11,12] The *t*-Se is formed inside the mesopores due to the absence of interchannel walls of $AlPO_4$-5 single crystals (a structural imperfection of the zeolite single crystal). The vibrational mode with low frequency (122 cm^{-1}) is assigned to the E_3-symmetric

(17) Ravy, S.; Launois, P.; Moret, R.; Pouget, J. P. *Z. Kristallogr.* **2005**, in press.

(18) Cochran, W.; Crick, F. H. C.; Vand, V. *Acta Crystallogr.* **1949**, *5*, 581.
(19) Ikawa, A. *J. Phys. Soc. Jpn.* **1994**, *63*, 1986−1994.

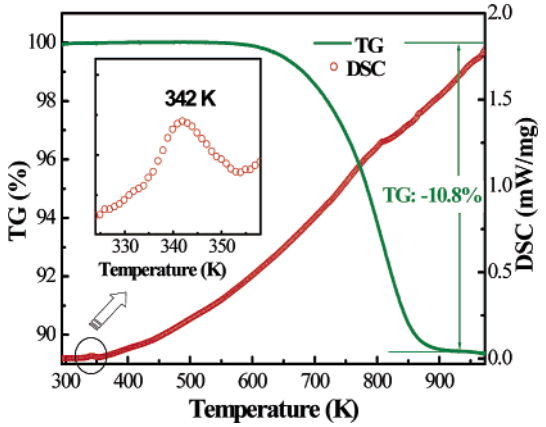

Figure 5. TG (—) and DSC (○) curves for Se/$AlPO_4$-5 samples in the temperature range 294−973 K. The inset shows the structure transformation temperature.

bending mode for the Se_8 ring, which is close to the theoretical calculations of 116 cm^{-1}.[20] The assignment of the Raman band in the range 450−550 cm^{-1} is complicated. The details will be described in section 3.3.3. In the *YY* configuration (both the excitation and the scattering light are perpendicular to the crystal axis *c*), only the E_3 (122 cm^{-1}) and A_1 (267 cm^{-1}) modes of the Se_8 ring are observed.

Nakamura et al. have calculated the phonon dispersion curves and vibrational spectra of the regular helical Se chain. The information needed for their calculations, i.e., the force constant matrix, dynamical-charge tensor, and polarizability-derivative tensor, were obtained from ab initio molecular orbital calculations with the second-order Møller−Plesset perturbation theory for a Se chain with finite length.[9] The calculated off-resonance Raman active mode in the *ZZ* configuration is 262 cm^{-1}, and the experimental peak (258 cm^{-1}) matches the theoretical calculation within 2%. The theoretical off-resonance one-phonon modes in the *YY* configuration are 136, 247, and 262 cm^{-1}. However, in the measured polarized Raman spectrum excited with 632.8 nm laser line, we observed only the E_3 (122 cm^{-1}) and A_1 (267 cm^{-1}) modes of the Se_8 ring. No peaks indicative of a Se single helix are observed in the *YY* configuration. This difference arises from the fact that the experimental value in the *ZZ* configuration is resonance enhanced, since the excitation laser energy is at the tail of the Se helix absorption edge. For both *t*-Se and Se single helix, the strong anisotropy of Raman modes in the *ZZ* and *YY* configurations arises from the resonant anisotropic absorption of the Se helices.[19]

3.2. Phase Stability. Figure 5 shows the TG and DSC curves measured in the temperature range of 294−973 K. The sample mass loss during heating is shown in the TG curve. In the experiment, we kept the samples in the vacuum and carefully dehydrated the samples at 380 K for several hours before we started the thermal measurement. After the dehydration, no mass loss was observed at temperatures below 500 K for the Se-loaded sample. When the temperature was increased above 550 K, the weight of the sample began to decrease significantly due to desorption of the Se species from the $AlPO_4$-5 channels. The mass loss was saturated at temperatures higher than 900 K; the weight loss was 10.8 wt %. Assuming that all the $AlPO_4$-5 channels are completely filled with Se specimens, then the weight ratio of Se to $AlPO_4$-5 should be about 29 wt % if all the Se specimens are from helical Se chains, and 23 wt % if only Se_8 rings were in the channels, which is smaller than the weight ratio of pure chain structure. The measured weight ratio of the saturated loaded sample is smaller than the calculated values, indicating that the $AlPO_4$-5 channels are only partially filled by Se specimen. This result is consistent with X-ray diffraction analysis.?

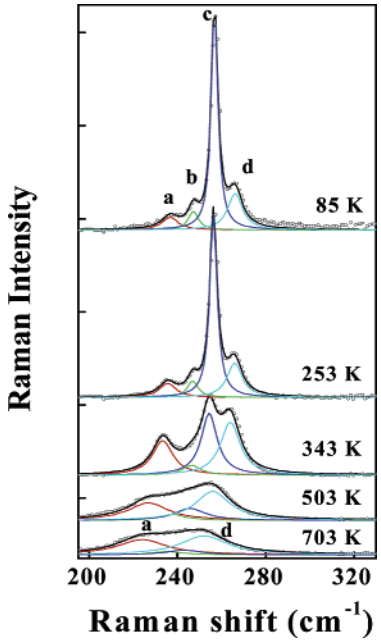

Figure 6. Vibrational spectra for a Se/$AlPO_4$-5 sample at different temperatures. All the spectra are well fitted by four Lorentzian lines.

In the DSC curve, an endothermic peak at 342 K is clearly observed, as shown in the inset in Figure 5, and at this temperature, no mass loss is observed. This endothermic peak is closely correlated to the structural transition of the loaded Se specimens. Usually, the endothermic process corresponds to the melting of crystalline samples. It is a first-order transition. It means that at the melting temperature, the sample absorbs heat and its temperature will not rise until all the sample has melted. Thus, the furnace has to put additional heat into the sample in order to melt the crystals and keep the temperature rising at the same rate as that of the reference pan. With increasing temperature, two endothermic processes occur: (1) desorption of enclosed Se species and (2) an endothermic process in the $AlPO_4$-5 framework. Since the weight ratio of Se to $AlPO_4$-5 crystal is around 1:10 (as indicated by the TG curve), the DSC curve in the high temperature range mainly is related to the endothermic process in the $AlPO_4$-5 framework.

Figure 6 shows the micro-Raman spectra for the Se/$AlPO_4$-5 sample measured at different temperatures. The sample temperature was altered using a Linkam THMS600 cooling−heating system. Each temperature point was kept for over 15 min before we recorded the spectra. There is a weak and broad photoluminescence background from the Se/$AlPO_4$-5 crystals. In the Raman spectra, we have subtracted the broad background.

As shown in Figure 6, at the low temperature of 85 K, the Raman signals are very sharp and can be clearly resolved into four peaks centered at 236, 247, 257, and 266 cm^{-1}, marked a, b, c, and d, respectively. Peak b corresponds to the vibrations of *a*-Se incorporated into the mesopores, which is not observed

(20) Goldbach, A.; Iton, L. E.; Saboungi, M.-L. *Chem. Phys. Lett.* **1997**, *281*, 69−73.

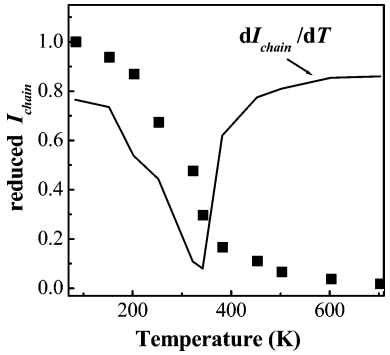

Figure 7. Temperature dependence of reduced intensity I_{chain}.

in the polarized Raman spectra at room temperature. The other three peaks are attributed to the symmetric bond-stretching A_1 modes of *t*-Se (peak a), isolated Se chains (peak c), and Se_8 rings (peak d). With increasing temperature, the four peaks show different behavior: The Raman intensity for peak a increases until room temperature is reached; the mode is softened and the line width increases as well. The Raman intensity for peak b decreases dramatically near 320−350 K. Peak c becomes softer and broader, and the intensity conspicuously decreases when the temperature is around 340 K. Peak d shifts to the low-frequency side, and the line width simultaneously increases, due to the thermal expansion effect (heating of the separated Se_8 rings induced lengthening of the molecular bond, and the bond force constant decreased, whcih led to the frequency shift and line width broadening). Previous experimental results showed that crystallization occurred in bulk *a*-Se when the temperature was increased. The crystallized cluster has been proved to be of trigonal form, which is stable at ambient. The crystallization temperature for bulk *a*-Se is about 380 K.[21] We observed a similar crystallization process for the *a*-Se in the mesopores: the Raman intensity of *t*-Se increased and the intensity of *a*-Se decreased. Although crystallization is an exothermic process, no corresponding peaks are observed in the DSC curve shown in Figure 5, since the density of *a*-Se in $AlPO_4$-5 mesopores is very low.

Figure 7 shows the temperature dependence of the reduction in intensity for the single chain, I_{chain}. The measured Raman intensity is reduced by dividing out $[n(\omega) + 1]$ to remove the population variations related to the temperature, where $n(\omega)$ is the Bose−Einstein factor, $n(\omega) = [\exp(\hbar\omega/kT) - 1]^{-1}$, and then normalized by the Raman intensity at 85 K. At low temperature, the change in intensity is small, meaning that only weak distortion happened in isolated chains. But when the temperature is around 340 K, the distortion of chains becomes very significant. In this case, the chains are in the torsion "melting" state, and the dihedral angles are totally different. The conspicuous discontinuity in the slope, as shown by the first derivative lines dI_{chain}/dT, indicates that a phase transition has occurred. The transformation temperature is estimated to be 337 K, which is comparable with the peaks observed in the DSC curve (342 K).

3.3. Electronic Properties. The electronic configuration of the Se atom is $4s^24p^4$. Two 4p electrons contribute to the covalent bond (σ) between neighboring Se atoms and form a helical chain structure. The remaining two 4p electrons are in lone-pair (LP) states that form the uppermost valence band, while the empty 4p antibonding states (σ^*) form the lowest conduction band. There is an energy gap between the LP and σ^* bands.[8] Most calculations agree on a direct gap with energy around 2.0 eV for *t*-Se. Slightly below the direct gap there occurs an indirect transition with energy around 1.8 eV.[1] It is known that the electronic properties of the bulk material will change dramatically when its dimension decreases to the nanometer size. In this section, we will report our investigations on the electronics and the electron−phonon coupling effect in an isolated Se helix using absorption and resonant Raman measurements

(21) Matsuishi, K.; Nogi, K.; Ohmori, J.; Onari, S.; Arai, T. *Z. Phys. D* **1997**, *40*, 530.

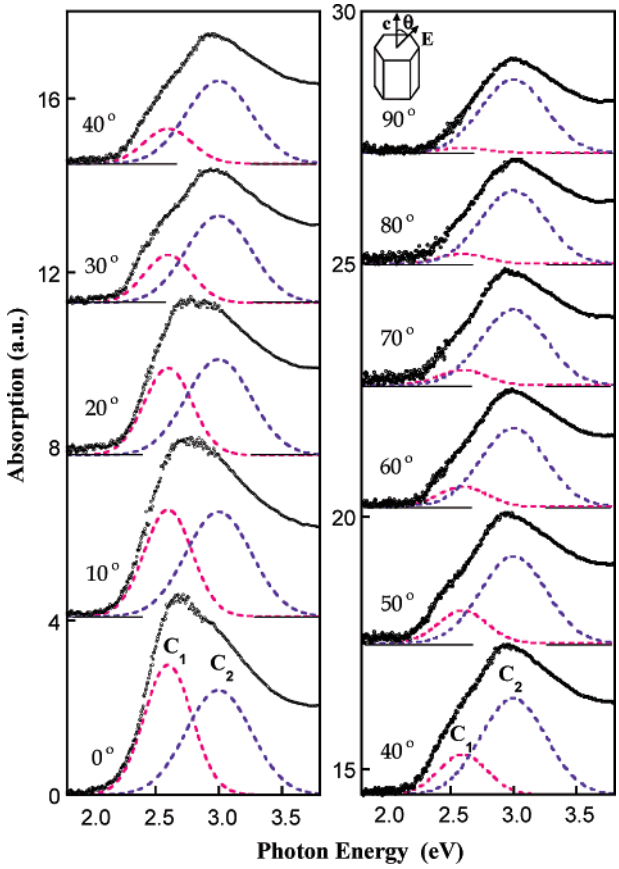

Figure 8. Polarized absorption spectra of $Se/AlPO_4$-5 at room temperature in the photon energy range of 1.8−3.8 eV. The polarization geometry of the measurement is shown in the inset.

3.3.1. Blue Shift in the Absorption Bands. To easily measure the absorption spectra, we fixed the sample in a hole drilled on a ceramic plate with epoxy resin. After the resin hardened, we polished the sample mechanically and then used Ar ion milling to as thin as 10 μm. The incident polarized light beam was focused onto the sample to a spot as small as 50 μm by using a reflecting objective. The transmitted light was collected by another conjugated reflecting objective. The signal was dispersed by a 275 mm monochromator before it was sent to the detector.

Figure 8 shows the absorption spectra of a $Se/AlPO_4$-5 single crystal measured at room temperature for the light polarized along different directions. The polarization geometry is shown in the inset of the figure. The absorption spectrum (open circles) for the light polarized parallel to the crystal axis ($\theta = 0°$, $E||c$) is shown at the bottom of the left column. The absorption spectrum can be decomposed into two bands with peak energy

at 2.6 and 3.0 eV (marked C_1 and C_2, respectively), as shown by the dashed curves. At $\theta = 0°$ polarization, the C_1 band dominates the spectrum. However, the amplitude of the band decreases monotonically with increasing the polarization angle, and finally becomes negligible at $\theta = 90°$ ($E \perp c$). In contrast, the C_2 band is less polarization dependent. The very different polarization behavior of the two bands indicates that they might originate from Se specimens of two different structures.

We assign the C_1 band to the absorption of helical Se chains, which is blue shifted about 0.6 eV from the direct-gap transition of the trigonal Se crystal. The blue shift can be qualitatively interpreted in terms of quantum confinement of an electron and a hole in a one-dimensional quantum wire, using the effective mass approximation.

If we assume that the Se chain has a cylindrical wire structure in the $AlPO_4$-5 channel, then the ground-state wave function of the electron and hole confined in the cylindrical quantum wire of radius R is

$$\phi_0(\rho) = \frac{J_0(\alpha_0 \rho/R)}{\sqrt{\pi} R J_1(\alpha_0)} \quad (1)$$

where $\alpha_0 = 2.405$ is the first zero of the Besssel function J_0 and ρ is the radial coordinate. The total energy of the confined electron−hole is given by the sum of kinetic, Coulomb, and matrix solvation energies, in which the kinetic energy is dominant in the present case and is given by[22]

$$E_0 = \alpha_0^2 \hbar^2 / 2m^* R^2 \quad (2)$$

where m^* is the reduced mass of the electron. For the *t*-Se, the reduced mass is $m_{||}^* = 0.73 m_0$,[23] and $m_\perp^*/m_{||}^* \approx 4$,[24] where m_0 is the bare electron mass, and || and $\perp$ are in reference to the chain axis of *t*-Se. Quantitatively, the calculated energy is about 2.65 eV for Se/$AlPO_4$-5 if we use the parameters $R = 3.6$ Å (from the XRD result) and $m_\perp^* \approx 2.92 m_0$, which is in good agreement with the experimental value of 2.6 eV.

The measured absorption energy (2.6 eV) of the Se chains in the $AlPO_4$-5 channels (channel diameter 0.73 nm) is higher than the 2.33 eV calculated for a free-standing Se chain,[6,19] which has a van der Waals diameter of 0.6 nm, but it is lower than those of Se chains confined in smaller channels of zeolite mordenite (MOR, free channels, elliptic cross section 0.67 nm × 0.7 nm) and cancrinite (CAN, channel diameter 0.59 nm). The lowest absorption energy of the Se chains is 2.8 eV in the MOR channels[25] and 2.9 eV in the CAN channels,[26] respectively. The C_1 band is strongly dependent on the polarization, due to the high degree of orientation of the Se chains in the $AlPO_4$-5 channels.

The C_2 band can be attributed to the absorption of Se_8 rings. The photon energy (3.0 eV) of the band is the same as that reported for Se_8 rings in spherical cages of zeolite Lind type A (LTA).[27] The absorption band is blue shifted about 0.5 eV from the lowest absorption band of crystallized α-monoclinic Se, which is due to the absence of intermolecular interactions of the isolated Se_8 rings in the $AlPO_4$-5 channels. The lower polarization dependence of the C_2 band absorption indicates that the Se_8 rings are randomly oriented in the $AlPO_4$-5 channels.

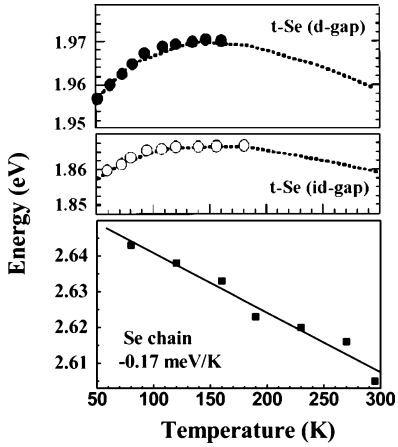

Figure 9. Lowest absorption energy of indirect gap (○) and direct gap (●) of *t*-Se and that of an isolated Se chain in the $AlPO_4$-5 channels (■), plotted as a function of temperature.

3.3.2. Temperature-Dependent Absorption Spectra. In *t*-Se, both direct and indirect transitions between LP and σ^* show abnormal temperature behavior: below 100 K the band-gap energies increase with increasing temperature due to the lattice dilation determined by acoustic phonons. Above 100 K, the electron−optical phonon interaction is increasingly important, leading to a bending of the temperature shift of the band-gap energies.[28]

We measured optical absorption spectra of Se/$AlPO_4$-5 crystals in the temperature range from 80 to 295 K. All the spectra are taken in the $E||c$ configuration. In Figure 9, the energy position of the absorption band C_1 for the Se helix (■) is plotted as a function of temperature. The temperature dependence of the indirect (○) and the first direct (●) absorption energies of *t*-Se is also shown in Figure 9.[28] The C_1 band decreases linearly as a function of increasing temperature, which is in sharp contrast to the temperature dependence of the absorption energy of *t*-Se, which has a positive temperature coefficient at the low-temperature region, with a bending of the temperature shift near room temperature. The absorption energy has a completely different temperature dependence for the isolated chain than for the *t*-Se crystal. This difference can be understood by considering the lattice dilation and electron−optical phonon coupling contributions to the absorption energy.

At temperature T, the gap energy of *t*-Se can be written as

$$E_g(T) = E_0 + E_p(T) + E_d(T) \quad (3)$$

where E_0 is the gap energy at zero temperature, E_p is the contribution of electron−optical phonon coupling in the absence of any distortion of the lattice, which leads to a decrease of the gap energy with increasing temperature, and E_d is the contribution of the lattice dilation. For *t*-Se crystals, the thermal-dilation-

(22) Banyai, L.; Galbraith, I.; Ell, C.; Haug, H. *Phys. Rev. B* **1987**, *36*, 6099−6104.
(23) Tutihasi, S.; Chen, I. *Phys. Rev.* **1967**, *158*, 623−630.
(24) Weiser, G.; Stuke, J. *Phys. Status Solidi (b)* **1971**, *45*, 691−703.
(25) Bogomolov, V. N.; Kholodkevich, S. V.; Romanov, S. G.; Agroskin, L. S. *Solid State Commun.* **1983**, *47*, 181−182.
(26) Bogomolov, V. N.; Efimov, A. N.; Ivanova, M. S.; Poborchii, V. V.; Romanov, S. G.; Smolin, Y. I.; Shepelev, Y. F. *Fiz. Tverdogo Tela* **1992**, *34*, 1722−1728.
(27) Parise, J. B.; MacDougall, J. E.; Herron, N.; Farlee, R.; Sleight, A. W.; Wang, Y.; Bein, T.; Moller, K.; Moroney, L. M. *Inorg. Chem.* **1988**, *27*, 221−228.
(28) Lingelbach, W.; Weiser, G. *Phys. Status Solidi (b)* **1975**, *70*, 461−469.

induced band-gap energy shift has three contributions and can be written as

$$\left(\frac{\partial E}{\partial T}\right)_{\mathrm{dil}} = \Xi_a \alpha_a + \Xi_c \alpha_c + \Xi_R \alpha_R \qquad (4)$$

where α_a, α_c, and α_R are the thermal expansion coefficients of the interchain distance a, the unit cell length c, and the helical chain radius R, respectively, and Ξ_i ($i = a, c, R$) is the corresponding deformation potential.

According to a model calculation based on a simple anharmonic approximation, the thermal dilation of the lattice is dominated by interchain acoustic phonons, and its effect is described by the first term in eq 4.[29] This term gives rise to a sizable increase of the gap energy with increasing temperature. The contributions to the temperature shift from the second term due to thermal dilation of c and from the third term due to the dilation of R are negative, while the second term is negligibly small. When the temperature is not very high, the population of the optical phonon is small and the temperature shift of the absorption energy is dominated by the thermal dilation. Thus, the positive temperature coefficient of the gap energy of *t*-Se results mainly from the large contribution of the thermal dilation due to interchain acoustic phonons. In the high-temperature region, the contribution of the electron−optical phonon coupling is increased, leading to a bending effect on the temperature dependence of the band-gap energy, as shown in Figure 9.

The helical Se chains in Se/$AlPO_4$-5 are isolated and the interchain interaction is expected to be much smaller because of the large distance (13.7 Å) between neighboring channels in $AlPO_4$-5. Hence, the thermal dilation due to the interchain acoustic phonons would no longer contribute to the temperature shift of the absorption energy in Se/$AlPO_4$-5. The total temperature coefficient of absorption energy for Se/$AlPO_4$-5 is then given by

$$\frac{\mathrm{d}E}{\mathrm{d}T} = \Xi_c \alpha_c + \Xi_R \alpha_R + \left(\frac{\partial E}{\partial T}\right)_{\mathrm{p}} \qquad (5)$$

where $(\partial E/\partial T)_{\mathrm{p}}$ is the temperature coefficient due to the electron−optical phonon coupling without lattice deformation.

The temperature shift of the lowest absorption energy due to the electron−acoustic phonon coupling (lattice dilation) is approximately a linear function of temperature, while the temperature shift due to the electron−optical phonon coupling is nonlinear with temperature.[28] The excellent linear decrease of the absorption energy with increasing temperature in Se/$AlPO_4$-5, shown in Figure 9, implies that the main contribution to the temperature shift of the isolated Se chain is due to lattice dilation, and the contribution from electron−optical phonon coupling is negligible. From the experimental data shown in Figure 9, the temperature coefficient of the lowest absorption energy is calculated to be −0.17 meV/K for Se/$AlPO_4$-5. This value is in good agreement with the value of −0.2 meV/K calculated from the first two terms of eq 5, which again supports the assertion that the temperature shift of the absorption energy is mainly due to the intrachain electron−acoustical phonon coupling and the electron−optical phonon coupling is negligibly small in the isolated chain system because of the weakening of the Frohlich coupling strength in low-dimensional systems.[30]

(29) Guenzer, C. S.; Bienenstock, A. *Phys. Rev. B* **1973**, *8*, 4655−4667.

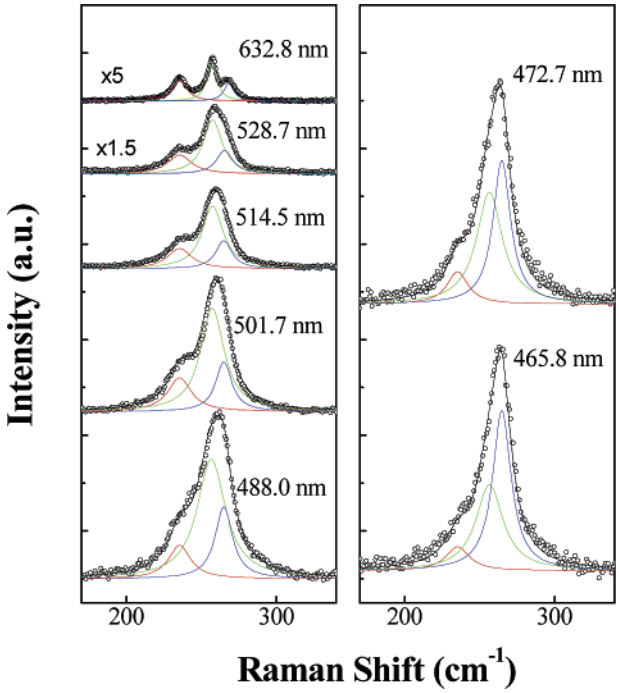

Figure 10. Representative spectra of a Se/$AlPO_4$-5 single crystal for seven different laser lines in the range 170−340 cm^{-1}. All the spectra are fitted by three Lorentzian line shapes.

3.3.3. Resonance Raman Spectra. Figure 10 shows representative Raman spectra of a Se/$AlPO_4$-5 single crystal for seven different laser energies in the range 170−340 cm^{-1}. All the signals were collected in the *ZZ* configuration. The weak broad photoluminescence from the sample was baseline corrected from the spectra. The spectra intensity is normalized to the laser power.

Since the *a*-Se is crystallized into *t*-Se at ambient temperature, we fit the spectra using only three Lorentzian spectral line shapes. As the excitation laser shifts toward shorter wavelength, the Raman scattering intensity increases, and the relative intensities for the three peaks are strongly dependent on the excitation laser energy. As shown in Figure 10, with decreasing laser wavelength, the Raman intensity for the Se single helix first increases and then decreases as the laser wavelength becomes lower than 473 nm. The Raman intensity for Se_8 rings increases monotonically with decreasing laser wavelength in our measurement range.

The integrated intensities of the Se single-helix A_1 mode (△) and Se_8 ring A_1 mode (☆) are plotted as a function of the excitation laser energy in Figure 11. The effect of the absorption coefficient has been corrected as described by Loudon,[31] in addition to the laser power normalization. The open triangles are well fitted by a Lorentzian line shape centered at 2.58 eV. The Raman signal is significantly enhanced for this particular energy, owing to the matching between the excitation energies and electronic transitions in the Se helix. This result is in good agreement with the polarized absorption measurement, which can manifest the electronic dipole transitions directly. The solid curve plotted in Figure 11 is the absorption spectrum for a Se/$AlPO_4$-5 single crystal with light polarized parallel to the crystal axis *c*. Thus, we can assign the resonance observed at 2.58 eV

(30) Tang, Z. K.; Nozue, Y.; Goto, T. *Mater. Sci. Eng. B* **1995**, *35*, 410−416.
(31) Loudon, R. *J. Phys. (Paris)* **1965**, *26*, 677−683.

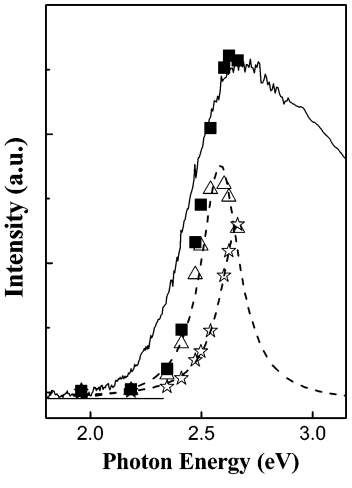

Figure 11. Integrated intensity of Se chain (△) and Se_8 rings (☆), plotted as a function of the excitation laser energy. The solid curve is the absorption spectrum of Se/$AlPO_4$-5 for the light polarized parallel to the crystal axis, and the solid squares are the sum of integrated intensities for the Se helix and Se_8 rings.

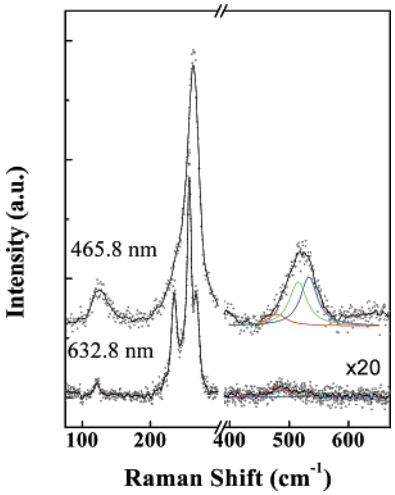

Figure 12. One-phonon and two-phonon Raman modes for a Se/$AlPO_4$-5 crystal with different excitation laser lines.

to the Se single helix. Since the absorption band for the Se_8 ring is at 3.0 eV, which is out of the photon energy measurement range, we could not show the complete resonance window for Se_8 rings. However, when the excitation laser energy approaches 2.66 eV, the Raman intensity for Se_8 ring increases monotonically, implying that the A_1 mode (☆) for the Se_8 ring is enhanced at higher excitation energy, and the peak for the resonance Raman effect should be higher than 2.66 eV. The solid squares shown in Figure 11 are the sum of integrated intensities for the Se single helix and Se_8 rings. The intensity profile for those points matches the absorption spectrum quite well.

Figure 12 shows the Raman spectra excited with 465.8 nm (2.66 eV) and 632.8 nm (1.96 eV) laser lines (○). The solid lines are the smoothed ones. Three Raman features dominate the spectra: the symmetric bond-stretching A_1 modes in the frequency range 200−340 cm^{-1} discussed above; the E_3-symmetric bending mode for the Se_8 ring (122 cm^{-1}), the scattering intensity of which is stronger when the excitation laser has higher energy; and vibrational modes in the range 450−550 cm^{-1}.

The feature in the high-frequency range is rather complicated: both the scattering intensity and the band center depend on the excitation energy. The band is centered around 489 cm^{-1} for low excitation energy (632.8 nm). It up-shifts to around 525 cm^{-1} for high excitation energy (465.8 nm), and its scattering intensity becomes stronger as well. We fit the spectra between 450 and 550 cm^{-1} by three Lorentzian lines, which are centered at 479, 516, and 534 cm^{-1}, respectively. These Raman shifts occur at twice the frequency shift of the first-order A_1 Raman lines of *t*-Se (236 cm^{-1}), Se single helix (258 cm^{-1}), and Se_8 ring (267 cm^{-1}). Thus, we can explain the Raman feature in the high-frequency region as the resonance enhancement in second-order Raman scattering. The second-order scattering is due to processes in which light has suffered two successive first-order Raman scatterings. It means two phonons participate in the process, and the final Raman shift is the sum of the individual frequency shifts. For low excitation energy (1.96 eV), the second-order scattering arises from the one-phonon modes of *t*-Se and the Se single helix. Since the excitation energy is in the tail of the absorption edge, the second-order scattering is relatively weak. As the laser energy is increased to 2.66 eV, which is close to the electronic transition energy for both the Se single helix and Se_8 rings, the second-order scattering becomes strong at frequencies 516 and 534 cm^{-1}, thus making the center of the total high-frequency shift from 489 to 525 cm^{-1}.

In conclusion, we have introduced isolated Se helices into the one-dimensional channels of $AlPO_4$-5 single crystals by a physical diffusion method and experimentally investigated the geometry, phase stability, and electronic and electron−phonon coupling properties of these Se chains. Single-crystal X-ray scattering experiments show diffuse planes perpendicular to c^* at $Q_z = 0$ and $Q_z \approx \pm 2\pi/6.45$ $Å^{-1}$, which correspond to the scattering from periodic Se chains with their long axis parallel to the direction c of the $AlPO_4$-5 channels. Possible parameters of the Se chain can be deduced from these experiments: interatomic distance $r \approx 2.38$ Å, bond angle $\theta \approx 121°$, and dihedral angle $\Psi \approx 42°$. Compared with the crystalline trigonal Se, the Se single-helical chain is considerably flexible due to the absence of interchain interactions. The phase stability of isolated Se chains has been studied by thermogravimetry, differential scanning calorimetry, and temperature-dependent micro-Raman measurements. The results show that Se single chains can convert from a weak distorted phase into another phase with strongly disordered structure ("melting" state) around 340 K, which confirms that the isolated Se chain is soft and can be easily altered by small perturbations.

The electronic properties of isolated Se chains have been investigated by recording polarized and temperature-dependent absorption spectra. Since the electrons are confined in the one-dimensional channels, the absorption band of the Se chain is obviously blue shifted compared with that of trigonal Se, and with increasing temperature, this band shifts to the lower energy side linearly, in sharp contrast to the nonlinear temperature coefficient in trigonal Se, which is attributed to the greatly diminished interchain interaction and the weakening of the electron−optical phonon coupling in a low-dimensional system. Electron−phonon coupling in Se chains confined in a

nanoporous matrix has been investigated by using resonant Raman spectroscopy performed with several different laser lines from deep blue to near-infrared. The spectra strongly depend on the energies of the excitation laser lines. The one-phonon symmetric A_1 mode for the Se single helix is enhanced in the vicinity of its absorption bands. Detailed analysis shows that the Raman band in the high-frequency range 450−550 cm^{-1} is composed of several individual second-order Raman bands for the confined Se species. These two-phonon Raman shifts occur at twice the frequency shift of the first-order Raman lines, and their intensities are also enhanced when the excitation laser energy matches an electronic transition in the Se species.

Acknowledgment. We thank Dr. H. D. Sun for his suggestions and help in measuring the absorption spectra. Financial support from RGC of Hong Kong through CERG, Guangdong Natural Science Foundation (5301084), National Natural Science Foundation of China (60471048), and Shenzhen STI foundation (200432) is appreciated.

JA053686+